Supplementary Information for 'Dynamic Modulation of Electronic Properties of Graphene by Localized Carbon Doping Using Focused Electron Beam Induced Deposition'

*Songkil Kim, Michael Russell, Mathias Henry, Steve S. Kim, Rajesh R. Naik, Andrey A. Voevodin, Seung Soon Jang, Vladimir V. Tsukruk, and Andrei G. Fedorov**

S1. Optimization of a graphene transfer method

The two factors determining graphene film quality upon transfer onto a SiO_2/Si substrate are wrinkles and cracks. While the cracks result from transfer procedures, the wrinkles can also originate from the roughness of graphene-supporting Cu foil during graphene growth. A high temperature (~1000 ◦C) condition for graphene growth results in long, straight line deformations of Cu foil.[S1] It ends up generating similarly shaped wrinkles on transferred graphene.[S1] It is unavoidable unless the low temperature condition is used for graphene growth. In this work, we only focused on the optimization of the graphene transfer procedure. Graphene transfer procedure results in cracks and wrinkles with random directions having microscale lengths with nanoscale heights.[S1] Unlike the long, straight line wrinkles coming from the Cu foil, those defects can be minimized *via* optimizing the transfer procedures.

The general PMMA-mediated wet transfer method is described in Figure S1. 4 w/w% PMMA solution in toluene is spin-coated on a graphene/Cu foil sample with 3000 rpm for ~ 1 min, which results in ~200 nm thickness of the coated PMMA layer. A PMMA/graphene/Cu foil sample is post-baked on a hot plate at 180 ◦C for ~ 1min, in order to evaporate the solvent and harden the PMMA layer. PMMA coating on graphene/Cu enables graphene to be visible after Cu etching and also lowers the possibility that graphene film is torn during the transfer procedures. Then, the sample is placed into 0.05 g/ml ammonium persulfate/DI water solution, which is an etchant of Cu. The Cu foil completely dissolves into the solution after ~3 hrs, and only the PMMA/graphene remains floating on the solution surface. By scooping it out of the solution with a SiO_2/Si substrate, the PMMA/graphene film is transferred onto the substrate. In order to remove water and establish better contact between the PMMA/graphene and the substrate before removing the PMMA layer, the sample is heated to 180 ◦C on a hot plate. Finally, the PMMA layer is removed using acetone heated to 80 ◦C, and the graphene film is washed several times using DI water to remove the residual solvent and solutes. This method is widely accepted for graphene transfer, but significant density of cracks can occur during removal of the PMMA layer.[S2] To overcome this problem, an improved transfer method (called 'improved PMMA-mediated wet transfer method') was developed adding an additional PMMA coating step to the transferred PMMA/graphene sample before removing the 1st PMMA layer.[S2] The

additional PMMA liquid was found to redissolute the 1st PMMA layer on graphene and mechanically relaxes the underlying graphene film, leading to a better contact with the SiO_2/Si substrate upon transfer and which, in turns, reduces the number and size of cracks.[S2]

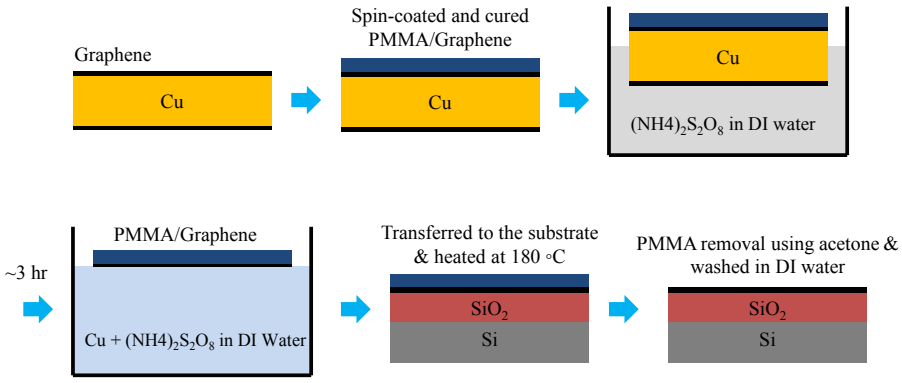

Figure S1. Schematic of the PMMA-mediated wet transfer method.

We first utilized the 'improved PMMA-mediated wet transfer method' to reduce the number of cracks. Figure S2(a) shows SEM images of graphene transferred onto the SiO_2/Si substrate. While some cracks are found on the graphene film, most area of the film is very continuous, and thus, can be utilized for electronic device fabrication. However, as shown in the AFM images (Figures S2(b) and S2(c)), the film quality and thickness are not uniform throughout, with a high density of micro-scale wrinkles, which may degrade the performance of graphene devices.

Figure S2. (a) SEM images of the graphene film transferred onto a 300 nm SiO_2/Si substrate, and AFM images of graphene in the areas with (b) the lowest and (c) the highest densities of wrinkles. The z-scale of AFM images is 50 nm.

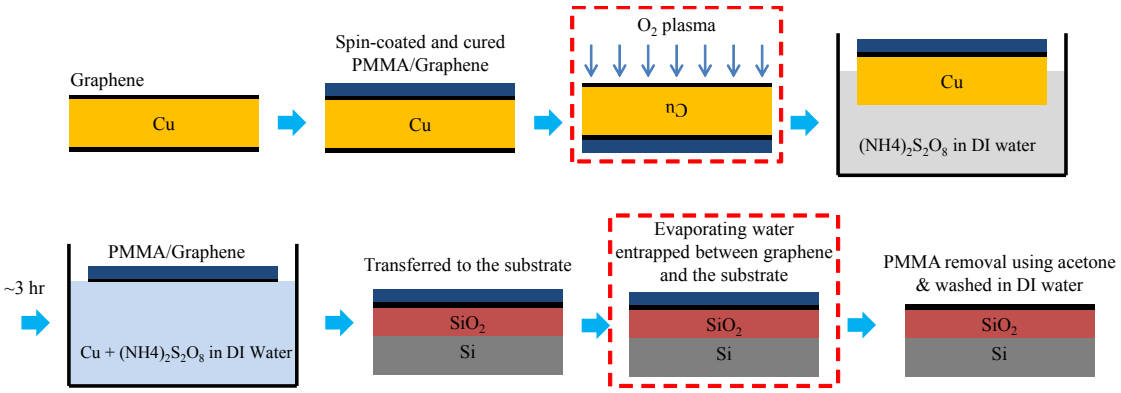

Figure S3. Schematic of the PMMA-mediated wet transfer method with additional steps of removing any graphene or carbon structures on the back side of Cu foil and carefully controlled slow evaporation of water entrapped between graphene and the substrate.

In order to achieve the better graphene quality, one additional step was added to the transfer procedure, along with investigating the effect of the water evaporation rate on the final outcome of the quality of graphene film, as shown in Figure S3. Graphene also grows on the back side of Cu foil, which is possibly detrimental to the quality of the film when it is transferred from copper to a device substrate. Thus, before dissolving the Cu foil, graphene present on the back side of Cu foil was etched away by exposing to O_2 plasma at the pressure of 50 mTorr for 40 s. Then, the Cu foil was cut into three pieces in order to study the effect of the water evaporation rate (controlled by changing the temperature of the PMMA/graphene transferred onto the SiO_2/Si substrate) on the transferred graphene film quality. Three different temperature conditions were considered when evaporating water after transferring PMMA/graphene onto the SiO_2/Si substrate. The PMMA/graphene samples were heated to (1) 180 °C for rapid evaporation, (2) 50 °C for intermediate evaporation, and (3) being tilted at room temperature so that water can flow out slowly from the space between the PMMA/graphene and the substrate. After plasma etching of graphene on the back side of Cu foil, all three films have uniform distribution of the wrinkles (height < 10 nm) and the thickness with 1.5 nm ~ 2.0 nm. Even at the intermediate evaporation rate, significant wrinkles can be seen on the graphene film (Figure S4(b)), comparable to those at the rapid evaporation rate (Figure S4(a)). However, when water is removed from a tilted sample at room temperature, the graphene film has been found to have much lower density of wrinkles (Figure S4(c)).

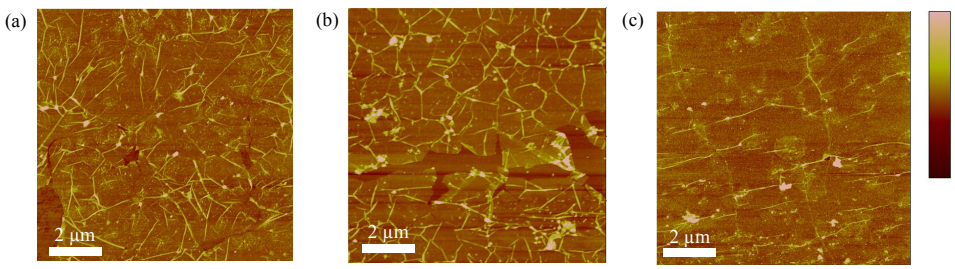

Figure S4. AFM images showing the distribution of wrinkles on the graphene films transferred onto the 300 nm SiO_2/Si substrates with (a) rapid evaporation (at 180 °C), (b) intermediate rate evaporation (at 50 °C) and (c) slow evaporation (tilted at room temperature) of water entrapped between PMMA/graphene and the SiO_2/Si substrates. The z-scale of the images is 20 nm.

Optical microscope images shown in Figure S5 also suggest the superiority of the tilted drying method in that it can significantly reduce the number of cracks. Figure S5(a) shows the graphene film transferred with an intermediate water evaporation rate (heated to 50 °C). A lot of cracks are found on the graphene film which is detrimental to have consistent, highly reliable performance of graphene-metal devices and interconnects. On the contrary, the graphene film transferred with the tilted drying method at a room temperature in Figure S5(b) has a much lower density of cracks, which enables us to fabricate high quality graphene devices.

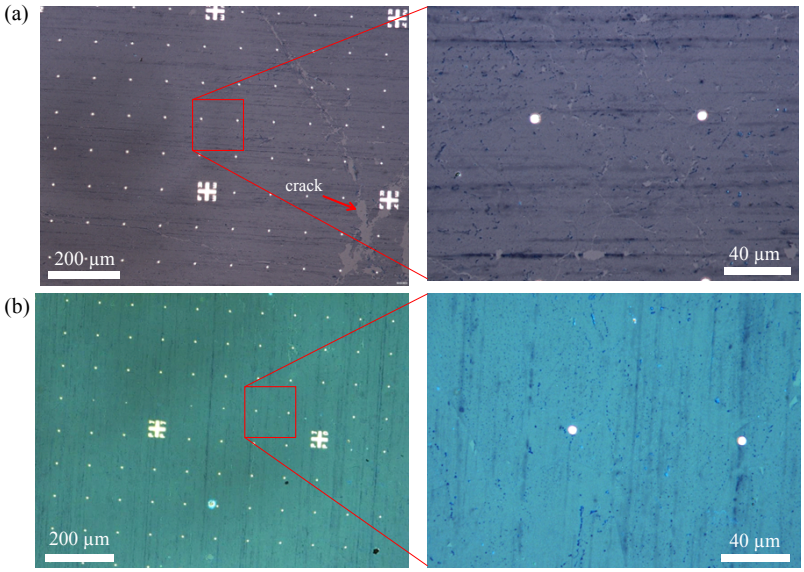

Figure S5. Optical microscope images of graphene films transferred with (a) intermediate evaporation rate (at 50 °C) and (b) slow evaporation rate (tilted at a room temperature) of water entrapped between PMMA/graphene and the 90 nm SiO_2/Si substrates, which shows the density of cracks generated during the transfer procedure.

The graphene film in Figure S5(b) was characterized for its structural quality (presence of defects on the graphene's hexagonal crystalline structure) using a confocal Raman spectroscopy, as shown in Figure S6. As explained previously, the structural quality can be evaluated with the intensity ratio of D to G peaks, I(D)/I(G), in the Raman spectrum. Smaller I(D)/I(G) represents fewer defects and a higher quality of graphene. I(D)/I(G) of the graphene film was found as ~0.18, which corresponds to the distance between two defects, L_D~ 26 nm and the number density of the defects ~ 464 /µm^2.[S3] The intensity ratio of 2D to G peaks indicates the number of graphene layers, along with a 2D peak shape.[S4] In the Raman spectrum, I(2D)/I(G) was found as ~2.5 and a 2D peak has a sharp single peak, indicative of a monolayer graphene.[S4] In conclusion, the PMMA-mediated graphene transfer process was successfully optimized to obtain a high quality monolayer graphene film on a SiO_2/Si substrate

for fabrication of graphene electronic devices, with minimal number and size of wrinkles and cracks which are inevitably generated during the transfer process.

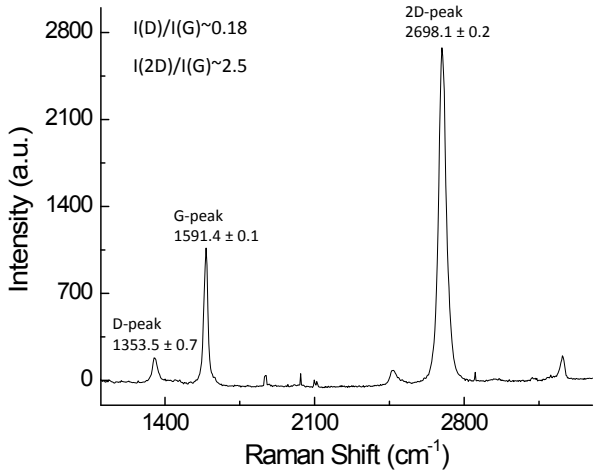

Figure S6. Raman spectrum of the graphene film in Figure S5(b), showing its structural quality and the number of graphene layers.

S2. Transfer characteristics of all the channels except the channel 1

Figures S7(a)~(e) show transfer characteristics of the channels from 2 to 6 in the graphene device shown in Figure 1, respectively. FEBID of carbon was conducted in exactly the same way to what was done in the channel 1 as described in Figure 2(a). All the channels have the same trend on the change of the transfer characteristics upon FEBID treatments. With a low electron dose, two peaks in the transfer characteristics appeared, indicating the presence of two different doping states (n-p-n junction formation) on the channels. After 72 hours (3 days) following the 1st FEBID treatment, the transfer characteristics recovered to that of a single doping state. After a long time (10 days), the transfer characteristics were stabilized with the overall reduced p-doping level of all graphene channels. Upon a follow-up high electron dose irradiation of a small area on metal electrodes, a uniform coverage of carbon deposits on the entire area of device channels has been established, resulting in a further negative shift of the Dirac voltage reaching almost near or below 0 V levels, depending on the channel lengths. Figure S7(f) shows the change of the averaged Dirac voltage obtained over measurements for all conduction channels 1 through 6, representing the effect of each processing step on Dirac point shifts. As shown in Figure S7(f), carbon doping of graphene leads to the reduced level of p-doping of graphene, with a complete switch to n-doping upon a high electron dose irradiation of metal contacts. It highlights the controls of a doping state of graphene using FEBID of carbon.

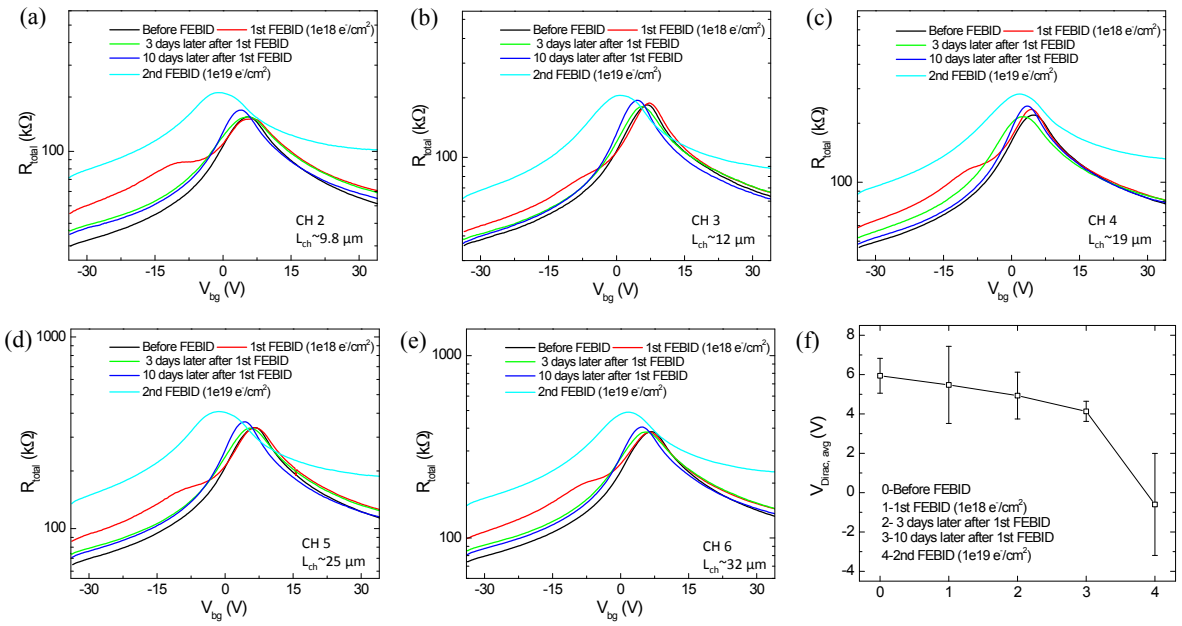

Figure S7. (a)~(e) Change of transfer characteristics of the channels from channels 2 to 6. (f) Multi-channel-averaged Dirac voltage change after FEBID treatment, indicating n-type doping of graphene with FEBID carbon on the channel.

S3. Raw data for electrical measurements of graphene devices

Figures S8(a) and S8(b) show raw data of drain-source current (I_{ds}) measured by sweeping a backgate voltage (V_{bg}) at a fixed drain-source voltage (V_{ds}=0.1 V) which were converted to device resistance based on Ohm's law as shown in Figures 2(b) and 3(b) of the manuscript, respectively.

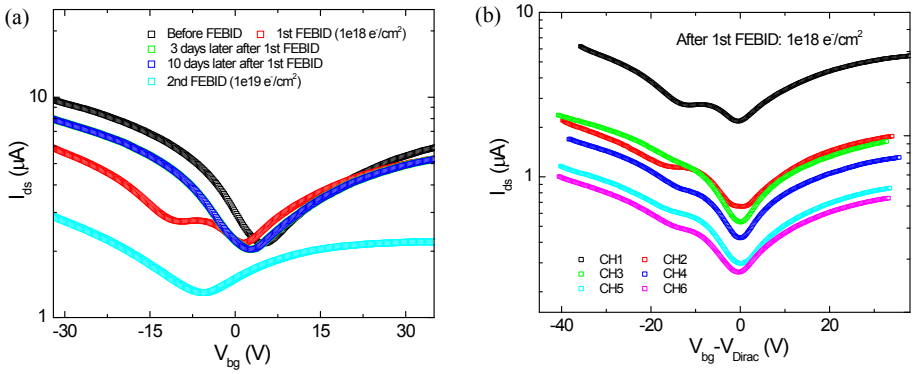

Figure S8. Measurement results of drain-source current *vs.* backgate voltage at a fixed drain-source voltage upon each process step.

S4. Topography images of Figure 4 and the corresponding transfer characteristics

Figure S9 shows AFM topography images and cross-sectional profiles of the graphene channel shown in Figure 4. Figure S9(a) shows the graphene channel before FEBID carbon deposition. After high energy electrons were irradiated on the left metal contact, a clearly visible, thick carbon film was formed only near the irradiated metal contact. After 6 hours following the FEBID treatment, the

carbon atoms migrated throughout the graphene channel resulting in more uniform film covering an entire channel. There is no distinguishable change in the topography image even after a long time (42 hours).

The change of the surface topology corresponds to the change of electrical transfer characteristics of the graphene device, as shown in Figure S10. Before FEBID, the graphene channel was heavily p-doped due to the interaction of graphene with uniformly distributed PMMA residues with an average thickness of ~3.8 nm. After the FEBID treatment, two distinct peaks can be found, which represents p-n junction formation. After 1 hour, two peaks in the transfer characteristic merged into a single broad peak with V_{Dirac}~0V, indicating a change of a doping state due to carbon diffusion and rearrangement. As time goes on, the single peak became sharper (more uniform carbon coverage and thus, more distinct single doping state) and stabilized with V_{Dirac}~10V after 6 hours. Finally, FEBID led to the significant negative shift (~Δ20V) of V_{Dirac} by converting PMMA residues to carbon.

To further confirm carbon diffusion and rearrangement as a driving mechanism for dynamic evolution of electronic properties of the graphene channel, a diffustion coefficient of clusted carbon atoms was estimated based on the time scale for dynamic evolution of the transfer characteristics following the relation, $D \sim L^2/t$, where D is a diffusion coefficient, L is a characteristic length scale (given by the graphene channel length ~8μm) and t is a characteristic time scale (taken as ~6 hours when the transfer characteristics reach the steady-state). This yields the diffusion coefficient ~ 3e-15 m^2/s. The estimated diffusion coefficient from our electrical measurement can be compared to predicted diffusion coefficient of carbon adatom on graphene obtained based on Density Functional Theory (DFT) calculation.[28] In DFT calculations, diffusion coefficient is calculated based on the equation, $D=v_0 a^2 \exp[-E_m/kT]$, where v_0 is a vibrational frequence of adatom, a is an elementary jump length, k is a Boltzman constant, T is temperature, and E_m is a migration barrier (~0.4 eV) for carbon adatom on graphene.[28] The DFT predicted diffusion coefficient at T=293 K is ~5.5e-15 m^2/s and it is an excellent agreement with our estimated value based on an approximate scaling analysis, which further strengthen our conclusion, based on experimental demonstrations, on the role of carbon diffusion and rearrangement on dynamic evolution of graphene electrical transfer characteristics.

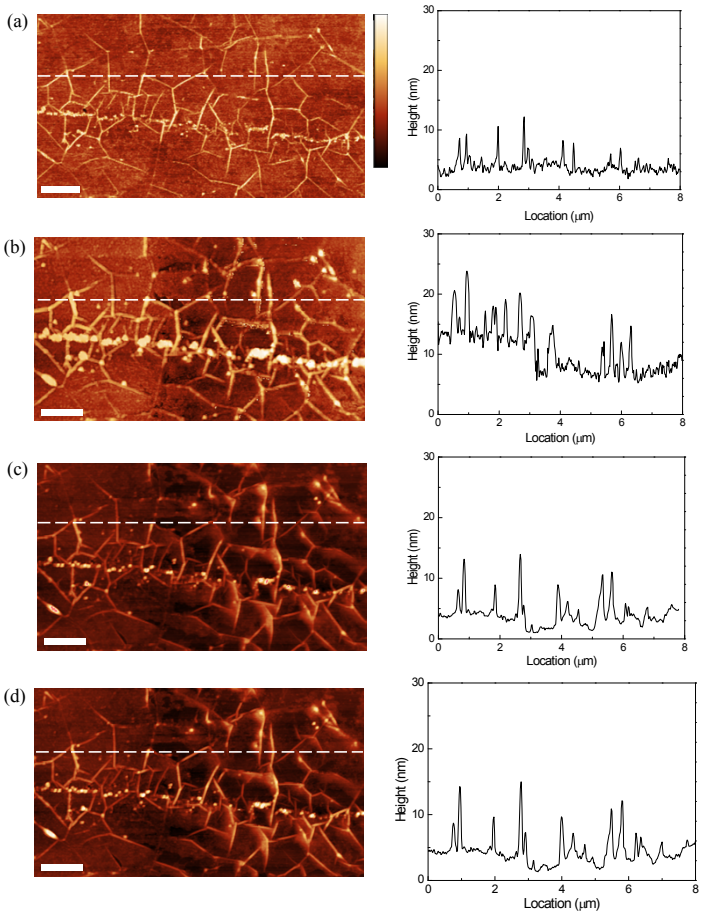

Figure S9. Topography images and cross-sectional profiles of the graphene channel in Fig. 4, measured using AFM, (a) before FEBID, (b) 4 hours, (c) 6 hours and (d) 42 hours after FEBID, respectively. Scale bar: 1 μm. Z-scale is 10 nm for (a) and 20 nm for others.

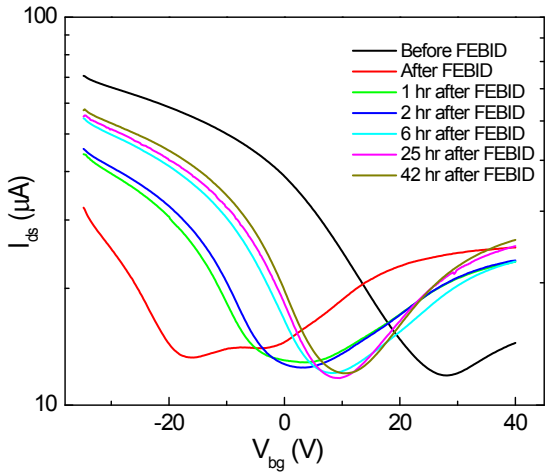

Figure S10. Change of the transfer characteristics of the graphene device, well explaining the effect of controllable FEBID carbon doping on the electronic properties of graphene, along with the change of the graphene surface topology and the phase images in the manuscript.

References

[S1]N. Liu, Z. Pan, L. Fu, C. Zhang, B. Dai and Z. Liu, *Nano Res*., 2011, **4**, 996.

[S2]X. Li, Y. Zhu, W. Cai, M. Borysiak, B. Han, D. Chen, R. Piner, L. Colombo and R. S. Ruoff, *Nano Lett*., 2009, **9**, 4359.

[S3]L. G. Cancado, A. Jorio, E. H. Martins Ferreira, F. Stavale, C. A. Achete, R. B. Capaz, M. V. O. Moutinho, A. Lombardo, T. S. Kulmala and A. C. Ferrari, *Nano Lett.*, 2011, **11**, 3190.

[S4]E. H. Martins Ferreira, M. V. O. Moutinho, F. Stavale, M. M. Lucchese, R. B. Capaz, C. A. Achete and A. Jorio, *Phys. Rev. B,* 2010, **82**, 125429.